First-Order Model Based Inductance Identification With Least Square Method for High-Speed Sensorless Control of Permanent Magnet Synchronous Machines

Yinfeng Hu, Kai Liu, Wei Hua, *Senior Member, IEEE*, and Mingjin Hu, *Student Member, IEEE*

***Abstract*—In sensorless control of high-speed permanent magnet synchronous machines (PMSMs), online inductance identification techniques can be employed to improve the position estimation precision. The high-order inductance identification model which is affected by the flux error, the dead-time effect equivalent voltage and initial rotor position error adopted in conventional methods often face challenges including robustness and accuracy. To address this issue, this article uses a first-order discrete-time model in the estimated $\gamma\delta$-frame to identify the winding inductance with disturbance injection. The first-order model allows the identification to be independent of flux error, initial rotor position error, and inverter nonlinearity, thus the robustness is improved. The proposed method takes the computational delay and discrete-time nature of pulsewidth modulation into account to avoid the model error brought by low ratio of carrier-to-fundamental-frequency. Additionally, the results are estimated by least square method to solve fluctuation problem caused by measurement noise and the possible surge phenomenon. Experiments are carried out on a high-speed surface-mounted PMSM for vacuum cleaner to verify the proposed method.**

***Index Terms*—First-order model, high-speed permanent magnet synchronous machines (PMSMs), inductance identification, least square method (LSM).**

I. Introduction

HIGH-SPEED permanent magnet synchronous machine (PMSM) has been widely utilized in air compressors and pumps for its high-power density and high efficiency [1], [2], [3]. In such applications, sensorless control is often employed because of space and weight requirements. However, for sensorless control of PMSM, the estimated rotor position error are dramatically influenced by the parameters of machine itself [4], [5], [6], [7], where the winding inductance has the most significant impact.

For mid- and high-speed operations, the back electromotive force (back EMF) observers are widely used to acquire rotor position information [8], [9], [10]. To deal with the time delay due to arithmetic calculation and pulsewidth modulation (PWM), one and a half sampling-period delay is compensated, thus the stability and dynamic performance can be improved [11]. However, these methods are derived in continuous-time domain. As the rotation speed increases, the ratio of carrier-to-fundamental-frequency is insufficient where the voltage under PWM cannot be approximated as a continuous signal. By modeling PWM as a zero-order holder (ZOH) voltage latch in stationary reference frame, the discrete-time model of high-speed PMSM is established for back-EMF observation and sensorless control with high performance is realized [12], [13].

Based on the above issue, various back EMF estimators are proposed based on the discrete-time PMSM model. Slide mode observer is used widely for simplicity [14]. For disturbance suppression, active disturbance rejection control, such as extended state observer (ESO), is applied [15]. Also, extended Kalman filter is introduced to address the nonlinear saturation problem [16]. Unfortunately, the aforementioned methods belong to model-based type and highly rely on accurate machine parameters including PM flux-linkage, winding inductance and resistance. Thus, the imprecise nominal values of machine parameters would degrade the performance of sensorless controlled high-speed PMSMs.

Previous research reveals that the rotor position estimation is influenced most significantly by the winding inductance [7], [17]. Thus, online identification of winding inductance is crucial for sensorless control of PMSMs where high-order models are usually employed [18], [19], [20]. Specifically, to avoid the mutual influence of parameter uncertainties, winding inductance is usually identified together with other parameters, such as rotor position error, resistance, flux-linkage and/or equivalent dead-time effect (DTE) voltage. In [18], the phase resistance and dq-axes inductances are identified, and then the rotor position error is obtained by recursive least square method (LSM). Further, to improve the identification accuracy, Zhu et

Manuscript received 7 September 2022; revised 20 January 2023 and 18 March 2023; accepted 23 March 2023. Date of publication 5 April 2023; date of current version 19 May 2023. This work was supported in part by the National Key Research and Development Program under Grant 2021YFB2500701 and in part by the Jiangsu Provincial Key Laboratory of Smart Grid Technology and Equipment, Southeast University under Grant 4216002101. Recommended for publication by Associate Editor E. Armando. *(Corresponding author: Wei Hua.)*

Yinfeng Hu, Kai Liu, and Wei Hua are with the School of Electrical Engineering, Southeast University, Nanjing 210096, China (e-mail: 230218868@seu.edu.cn; kliu@seu.edu.cn; huawei1978@seu.edu.cn).

Mingjin Hu is with the Southeast University, Nanjing 210096, China (e-mail: hmj@seu.edu.cn).

Color versions of one or more figures in this article are available at https://doi.org/10.1109/TPEL.2023.3263518.

Digital Object Identifier 10.1109/TPEL.2023.3263518

al. [21] suggest to compensate the voltage source invertor nonlinearity including DTE and equivalent on-resistance of power switches.

In high-speed machines, the ratio of carrier-to-fundamental-frequency is usually low, and the inductance is usually very small. Thus, DTE is hard to compensate because of the difficulty in zero-crossing detection brought by the relatively huge current ripple [10], [12], [13], [14], [15]. Wang et al. [20] propose a new multiparameter identification method to simultaneously estimate the phase resistance, flux linkage, inductance and the equivalent DTE voltage by using Gauss-Newton iteration. In [19], rotor position error and phase resistance are identified with minimum current vector online tracking based on a second-order model. Li and Kennel [22] utilize a dual Kalman filter to identify the phase resistance, flux linkage and equivalent DTE voltage. Experiments show that the application of parameter estimation method helps to improve the identification accuracy. In those literatures, multiple parameters are identified simultaneously because of the coupling of parameter uncertainty. Otherwise errors could be passed from one parameter to others during calculation. Nevertheless, the rank-deficient problem or ill-condition problem of such high-order model could bring problems in robustness and convergence [21].

What is more important, the above identification methods are all based on the continuous model, which are not suitable for high-speed PMSMs. In terms of rotor position compensation for sensorless control, separate identification of inductance could avoid rank-deficient problem theoretically. Recently, a discrete-time model based inductance calculation method is proposed [17]. With high signal to noise ratio (SNR), the amplitude of injected γ-axis current is less than 3% of δ-axis current. However, the error of inductance nominal value is obtained instead of directly identifying the real inductance value. As a result, the estimation method such as LSM is uneasy to be applied. Parameter estimation is important to maintain the accuracy of identification in the case of surge for air compressor. Previous experiments show that only hundreds of rpm of speed fluctuation can increase the identification error to more than 10%. In summary, an identification method independent of other uncertainties and robust to speed fluctuation is crucial.

To solve the above issue, a first-order model based on disturbance injection is proposed in this article to identify winding inductance and improve the precision of rotor position estimation. First, a high-speed PMSM model considering the computational delay and PWM effect is analyzed. Second, disturbance is injected to establish a first-order identification model (FOIM), which can be independent of PM flux linkage, rotor position error as well as the equivalent DTE voltage. Also, since no estimated variables, e.g., back-EMF, are used, the FOIM is irrelevant to sensorless algorithm. Consequently, the above characteristics guarantee the robust performance. Further, parameter estimation method known as the recursive auto-regressive LSM (ALSM) with forgetting factor is applied to solve the results fluctuation caused by measurement noise and possible surge of air compressors.

The rest of this article is organized as follows: The discrete-time model and the ESO-based sensorless control of a surface-mounted PMSM (SPMSM) is introduced in Section II. In Section III, an FOIM is deduced and proposed by disturbance injection. Then, the FOIM is mathematically and numerically proved to be unaffected from other parameter uncertainties, namely, the DTE, PM flux linkage and back-EMF. Finally, for improved performance in convergence, a recursive ALSM with forgetting factor is employed to solve the results fluctuation. In Section IV, experiments are carried out on a 60 000 r/min SPMSM. Finally, conclusion is drawn in Section V.

II. Discrete-Time Sensorless Control of SPMSM

A. Discrete-Time Model of SPMSM

In the synchronous reference frame, the continuous-time voltage equation of a SPMSM yields

$$\begin{cases} u_d^* + u_{\text{dead\_}d} = R_s i_d + L_s \frac{di_d}{dt} - i_q \omega L_s \\ u_q^* + u_{\text{dead\_}q} = R_s i_q + L_s \frac{di_q}{dt} + i_d \omega L_s + e_q \end{cases} \tag{1}$$

where $e_q = \omega\psi_m$, R_s is phase stator resistance, L_s is phase stator inductance, ψ_m is d-axis PM flux-linkage, ω is electrical angular velocity, and $u_{\text{dead\_}d}/u_{\text{dead\_}q}$ are the voltage distortions caused by DTE in d- and q-axes, respectively.

For PWM-based voltage-source inverter (VSI) fed to the SPMSM, the PWM effect is often modeled as a ZOH voltage latch [12], [15], [23]. Hence, (1) is discretized as

$$\begin{aligned} \boldsymbol{i}_{dq}(k+1) = H_d\left[\boldsymbol{u}_{dq}^*(k-1) + e^{j\omega T_s}\boldsymbol{u}_{\text{dead}_{dq}}(k)\right] \\ + G\boldsymbol{i}_{dq}(k) + H_e\boldsymbol{e}_{dq}(k) \end{aligned} \tag{2}$$

where the symbol (k-1), (k), (k+1) stand for the time $t = (k\text{-}1)T_s$, $t = kT_s$, $t = (k+1)T_s$ and T_s is the sampling period, and the three coefficients yield

$$G = e^{-\left(\frac{R_s}{L_s}+j\omega\right)T_s}$$

$$H_d = \frac{1}{L_s}\int_0^{T_s} e^{-\left(\frac{R_s}{L_s}+j\omega\right)\tau} e^{-j\omega(T_s-\tau)}d\tau = \frac{1-e^{-\frac{R_s}{L_s}T_s}}{R_s} e^{-2j\omega T_s}$$

$$H_e = -\frac{1}{L_s}\int_0^{T_s} e^{-\left(\frac{R_s}{L_s}+j\omega\right)\tau}d\tau = -\frac{1-e^{-\left(\frac{R_s}{L_s}+j\omega\right)T_s}}{R_s + j\omega L_s}. \tag{3}$$

The output voltage of inverter can be calculated using the last reference of $\boldsymbol{u}_{dq}{}^*$ as

$$\boldsymbol{u}_{dq}(k) = \boldsymbol{u}_{dq}^*(k-1)\, e^{-j\omega T_s} + \boldsymbol{u}_{\text{dead}_{dq}}(k). \tag{4}$$

For simplicity, complex vectors are used and $\boldsymbol{x_{dq}} = \boldsymbol{x_d} + \mathbf{j}\boldsymbol{x_q}$. The dq-axes frame is normally transformed to the $\gamma\delta$-axes frame in the sensorless control, which aligns with the estimated rotor position, and the transformation is

$$\boldsymbol{f}_{\gamma\delta} = T_{dq\to\gamma\delta}\boldsymbol{f}_{dq},\ T_{dq\to\gamma\delta} = e^{j\tilde{\theta}} \tag{5}$$

where $\boldsymbol{f}$ represents the variables, such as currents, voltages and back-EMFs, $\tilde{\theta} = \theta - \hat{\theta}$ is the rotor position error, θ is the real rotor position, and $\hat{\theta}$ is the estimated rotor position.

The relationship between the dq-axes and $\gamma\delta$-axes reference frames is shown in Fig. 1. Therefore, the discrete-time model of the SPMSM in the $\gamma\delta$-frame is

$$\begin{aligned} \boldsymbol{i}_{\gamma\delta}(k+1) = H_d\left[\boldsymbol{u}_{\gamma\delta}^*(k-1) + e^{j\omega T_s}\boldsymbol{u}_{\text{dead}_{\gamma\delta}}(k)\right] \\ + G\boldsymbol{i}_{\gamma\delta}(k) + H_e\boldsymbol{e}_{\gamma\delta}(k). \end{aligned} \tag{6}$$

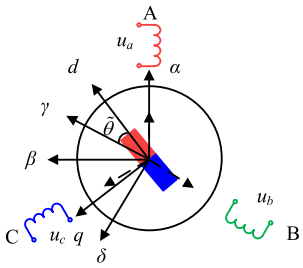

Fig. 1. Relationship between the dq-axes and $\gamma\delta$-axes reference frames.

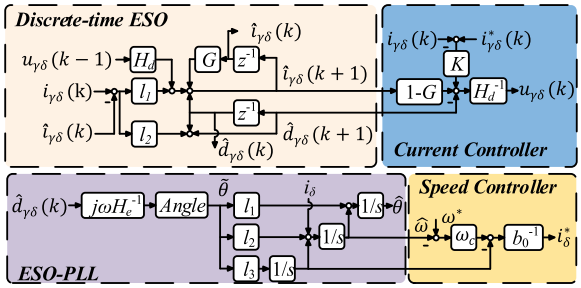

Fig. 2. ESO-based sensorless control structure of a SPMSM drive.

By comparing (1) and (6), the digital delay and PWM effect in the discrete-time model are accounted, which is neglected in the continuous-time model, resulting in an ideal sinusodual output voltage. The error caused by the above approximation is acceptable at low-speed, but can be problematic at high-speed by degrading the sability and dynamic of drives [12], [24], [25].

B. Structure of ESO

Fig. 2 shows the sensorless scheme utilized in this article. A discrete-time ESO is used for back EMF observation [15]

$$\begin{bmatrix} \hat{\boldsymbol{i}}_{\gamma\delta}(k+1) \\ \hat{H}_e\hat{\boldsymbol{e}}_{\gamma\delta}(k+1) \end{bmatrix} = A\begin{bmatrix} \hat{\boldsymbol{i}}_{\gamma\delta}(k) \\ \hat{H}_e\hat{\boldsymbol{e}}_{\gamma\delta}(k) \end{bmatrix} + B\left[\boldsymbol{u}^*_{\gamma\delta}(k-1) + e^{j\omega T_s}\boldsymbol{u}_{\mathrm{dead}_{\gamma\delta}}(k)\right] + L\left(\boldsymbol{i}_{\gamma\delta}(k) - C\begin{bmatrix} \hat{\boldsymbol{i}}_{\gamma\delta}(k) \\ \hat{H}_e\hat{\boldsymbol{e}}_{\gamma\delta}(k) \end{bmatrix}\right) \quad (7)$$

where $\hat{\boldsymbol{i}}_{\gamma\delta}$ are the estimated $\gamma\delta$-axes currents and $\hat{\boldsymbol{e}}_{\gamma\delta}$ are the estimated $\gamma\delta$-axes back-EMFs

$$A = \begin{bmatrix} \hat{G} & 1 \\ 0 & 1 \end{bmatrix}, B = \begin{bmatrix} \hat{H}_d \\ 0 \end{bmatrix}, C = \begin{bmatrix} 10 \end{bmatrix}, L = \begin{bmatrix} l_1 \; l_2 \end{bmatrix}. \quad (8)$$

Subtracting (6) from the first row of (7), the estimated current error is

$$\tilde{\boldsymbol{i}}_{\gamma\delta}(k+1) = \hat{G}\tilde{\boldsymbol{i}}_{\gamma\delta}(k) + \hat{H}_e\hat{\boldsymbol{e}}_{\gamma\delta}(k) - H_e\boldsymbol{e}_{\gamma\delta}(k) - \left(\hat{G}-G\right)\boldsymbol{i}_{\gamma\delta}(k) - \left(\hat{H}_d - H_d\right)\left[\boldsymbol{u}^*_{\gamma\delta}(k-1) + e^{j\omega T_s}\boldsymbol{u}_{\mathrm{dead}_{\gamma\delta}}(k)\right] \quad (9)$$

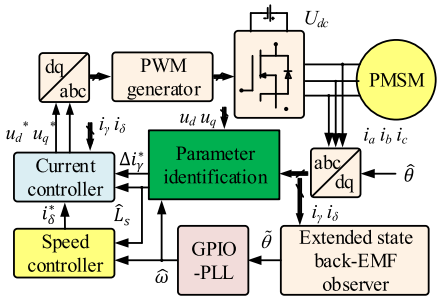

Fig. 3. PMSM sensorless control system with parameter identification.

where $\tilde{\boldsymbol{i}}_{\gamma\delta}$is the estimated current error in $\gamma\delta$-axes, and $\hat{H}_e$, $\hat{G}$ and $\hat{H}_d$ are the coefficients with the nominal values.

The current controller is designed by the machine transfer functions G and H, and the current error gain K is designed with the bandwidth needed. An ESO-based PLL is employed for fast response and zero-steady state error of the estimated rotor position. However, the estimated back EMF and rotor position will deviate from real values with parameter errors.

Obviously, as the current estimation error converges to zero, the estimated back EMF can be expressed as

$$\hat{\boldsymbol{e}}_{\gamma\delta}(k) = -\hat{H}_e^{-1}\left\{H_e\boldsymbol{e}_{\gamma\delta}(k) - \left(\hat{G}-G\right)\boldsymbol{i}_{\gamma\delta}(k) - \left(\hat{H}_d - H_d\right)\left[\boldsymbol{u}^*_{\gamma\delta}(k-1) + e^{j\omega T_s}\boldsymbol{u}_{\mathrm{dead}_{\gamma\delta}}(k)\right]\right\} \quad (10)$$

where $\hat{e}_\gamma = 0$ when the back EMF observer is at steady state.

III. First-Order Identification Model

In this section, sensorless control is realized with a parameter identification subsystem where an FOIM is deduced and applied. In Fig. 3, the current and speed controllers work at sampling frequency while the parameter identification subsystem is started manually. When identification begins, the γ-axis disturbance current reference is sent to the current controller and the response current and voltage information is recorded to calculate the real value of inductance. Then, the calculation result is transferred and updated in speed and current controllers.

A. Disturbance Injection Based on Discrete-Time Model

Comparing (6), (3), and (1), the term of back EMF only exists in the q-axis voltage equation in the continuous-time model, while in the discrete time model it is multiplied by a complex number H_e. Hence, in the continuous-time model (1), the identification of inductance can be achieved by only using the d-axis voltage equation, avoiding the back EMF term.

However, in the discrete-time model, as shown in (6), the back EMF term appears both in γ- and δ-axes voltage equations, which means the PM flux linkage and winding inductance must be identified simultaneously if the voltage equations are directly used. Thus, the identification becomes at least a second-order one. Further, if DTE is considered, there are four parameters needed to be identified, namely, equivalent DTE voltage V_{dead},

inductance L_s and PM flux linkage ψ_m and winding resistance R_s. So the (6) becomes a rank-deficient one even with the disturbance current injected [26]. Such a problem of high-order model brings difficulty in convergence.

To obtain a first-order model, disturbance is injected into the discrete-time model (6). The FOIM is obtained as followed.

1) Adding a small disturbance into (6). The magnitudes of disturbance injected should be much smaller than the magnitudes of i_δ. The frequency of injected disturbance signal should be much lower than the switching frequency to ensure the response can be easily separated and obtained. In this article, the injected current is smaller than 10% of the δ-axis current and the injected disturbance is a dc signal in $\gamma\delta$-frame. After the injection, the current equation at steady state is

$$\boldsymbol{i}_{\gamma\delta 2} = G\boldsymbol{i}_{\gamma\delta 2} + H_d\left(\boldsymbol{u}^*_{\gamma\delta 2} + e^{j\omega T_s}\boldsymbol{u}_{\mathrm{dead}_{\gamma\delta 2}}\right) + H_e\boldsymbol{e}_{\gamma\delta 2} \tag{11}$$

where, $\Delta\boldsymbol{i}_{\gamma\delta}$, $\Delta\boldsymbol{u}^*{}_{\gamma\delta}$, and $\Delta\boldsymbol{e}_{\gamma\delta}$ are the small disturbances and responses of currents, voltage and back EMF. In high speed operation, the speed fluctuation is very small, so the rotation speed is seen as a constant. The subscript "1" stands for the variable in the $\gamma\delta$-axis before injection and the subscript "2" stands for the variable in the $\gamma\delta$-axis after injection

$$\begin{aligned}
\boldsymbol{e}_{\gamma\delta 2} &= \Delta\boldsymbol{e}_{\gamma\delta} + \boldsymbol{e}_{\gamma\delta 1} = \boldsymbol{e}_{\gamma\delta 1}e^{j\Delta\tilde{\theta}}\\
\boldsymbol{i}_{\gamma\delta 2} &= \boldsymbol{i}_{\gamma\delta 1} + \Delta\boldsymbol{i}_{\gamma\delta}\\
\boldsymbol{u}^*_{\gamma\delta 2} &= \boldsymbol{u}^*_{\gamma\delta 1} + \Delta\boldsymbol{u}^*_{\gamma\delta}\\
\boldsymbol{u}_{\mathrm{dead}_{\gamma\delta 2}} &= \boldsymbol{u}_{\mathrm{dead}_{\gamma\delta 1}} + \Delta\boldsymbol{u}_{\mathrm{dead}_{\gamma\delta}}
\end{aligned} \tag{12}$$

where

$$\begin{aligned}
\Delta\tilde{\theta} &= \hat{\theta}_2 - \hat{\theta}_1 = \left(\hat{\theta}_2 - \theta\right) - \left(\hat{\theta}_1 - \theta\right)\\
&= \tilde{\theta}_1 - \tilde{\theta}_2
\end{aligned} \tag{13}$$

and $\tilde{\theta}_1, \tilde{\theta}_2$ stand for position errors before and after disturbance.

Thus, (11) becomes

$$\begin{aligned}
\boldsymbol{i}_{\gamma\delta 1} + \Delta\boldsymbol{i}_{\gamma\delta} = {} & G\left[\boldsymbol{i}_{\gamma\delta 1} + \Delta\boldsymbol{i}_{\gamma\delta}\right] + H_d\left[\boldsymbol{u}^*_{\gamma\delta 1} + \boldsymbol{u}_{\mathrm{dead}_{\gamma\delta 1}}\right]\\
& + H_d\left[\Delta\boldsymbol{u}^*_{\gamma\delta} + \Delta\boldsymbol{u}_{\mathrm{dead}_{\gamma\delta}}\right] + H_e\left[\boldsymbol{e}_{\gamma\delta 1}e^{j\Delta\tilde{\theta}}\right].
\end{aligned} \tag{14}$$

1) By subtracting (6) from (14)

$$\begin{aligned}
\Delta\boldsymbol{i}_{\gamma\delta} = {} & G\Delta\boldsymbol{i}_{\gamma\delta} + H_d\left[\Delta\boldsymbol{u}^*_{\gamma\delta} + \Delta\boldsymbol{u}_{\mathrm{dead}_{\gamma\delta}}\right]\\
& + H_e\left(\boldsymbol{e}_{\gamma\delta}e^{j\Delta\tilde{\theta}} - \boldsymbol{e}_{\gamma\delta}\right).
\end{aligned} \tag{15}$$

Equation (15) still contains the back-EMF term, which means the model may be affected by flux-linkage error.

B. Analysis on Back-EMF Disturbance Term

Since the back EMF term is associated with the estimated position error $\tilde{\theta}$, the analytical expression of $\tilde{\theta}$ is deduced. Assuming the system is at steady state, then the equation is

$$\boldsymbol{i}_{\gamma\delta} = \hat{G}\boldsymbol{i}_{\gamma\delta} + \hat{H}_d\boldsymbol{u}_{\gamma\delta} + \hat{H}_e\hat{\boldsymbol{e}}_{\gamma\delta}. \tag{16}$$

So, the estimated back-EMF can be calculated as

$$\hat{\boldsymbol{e}}_{\gamma\delta} = -\hat{H}_e^{-1}\left(\hat{G} - 1\right)e^{-j\tilde{\theta}}\boldsymbol{i}_{dq} - \hat{H}_e^{-1}\hat{H}_d e^{-j\tilde{\theta}}\boldsymbol{u}_{dq}. \tag{17}$$

Substituting (2) into (17), it yields

$$\begin{aligned}
\hat{\boldsymbol{e}}_{\gamma\delta} = {} & -\hat{H}_e^{-1}\left(\hat{G} - 1\right)e^{-j\tilde{\theta}}\boldsymbol{i}_{dq}\\
& - \hat{H}_e^{-1}\hat{H}_d e^{-j\tilde{\theta}}H_d^{-1}\left[(G-1)\,\boldsymbol{i}_{dq} + H_e\boldsymbol{e}_{dq}\right]\\
= {} & e^{-j\tilde{\theta}}\left[-\hat{H}_e^{-1}\left(\hat{G} - 1\right)\left(1 - \hat{H}_d H_d^{-1}\right)\right.\\
& \left.\boldsymbol{i}_{dq} + \hat{H}_e^{-1}H_e\hat{H}_d H_d^{-1}\boldsymbol{e}_{dq}\right].
\end{aligned} \tag{18}$$

Denote (18) as

$$\begin{aligned}
\hat{\boldsymbol{e}}_{\gamma\delta} &= e^{-j\tilde{\theta}}\left[-\hat{H}_e^{-1}\left(\hat{G} - 1\right)\left(1 - \hat{H}_d H_d^{-1}\right)\boldsymbol{i}_{dq}\right.\\
&\quad \left. + \hat{H}_e^{-1}H_e\hat{H}_d H_d^{-1}\boldsymbol{e}_{dq}\right]\\
&= e^{-j\tilde{\theta}}E.
\end{aligned} \tag{19}$$

Because $\hat{e}_\gamma = 0$ [14], [15], the argument of the E must be $\frac{\pi}{2} + \tilde{\theta}$. Thus

$$\begin{aligned}
\frac{\pi}{2} + \tilde{\theta} = {} & \arg(E) = \arg\left(\hat{R}_s + j\omega\widehat{L_s}\right)\\
& + \arg\left[\left(1 - \frac{1-\hat{x}}{\hat{R}_s}\frac{R_s}{1-x}\right)\boldsymbol{i}_{dq}\right.\\
& \left. - \frac{1-\hat{x}}{\hat{R}_s}\frac{R_s}{1-x}\frac{1}{R_s + j\omega L_s}\frac{1 - e^{-j\omega T_s}x}{1 - e^{-j\omega T_s}\hat{x}}\boldsymbol{e}_{dq}\right]
\end{aligned} \tag{20}$$

where x is for $e^{-R_s T_s/L_s}$ and with Taylor expansion

$$\begin{aligned}
\frac{\pi}{2} + \tilde{\theta} = {} & \arg(\hat{R}_s + j\omega\hat{L}_s) + arg\left[\frac{\hat{L}_s - L_s}{\widehat{L_s}}\boldsymbol{i}_{dq}\right.\\
& \left. - \frac{L_s}{\hat{L}_s}\frac{1}{R_s + j\omega L_s}\frac{1 - e^{-j\omega T_s}x}{1 - e^{-j\omega T_s}\hat{x}}\boldsymbol{e}_{dq}\right]\\
= {} & \arg\left(\hat{R}_s + j\omega\hat{L}_s\right) + \arg\left[E_2\right].
\end{aligned} \tag{21}$$

Then, the change of estimated rotor position error due to disturbance signal can be calculated by (13) and (21)

$$\Delta\tilde{\theta} = \arg(E_2) - \arg(E_2') = \mathrm{atan}\frac{\mathrm{Im}(E_2)}{\mathrm{Re}(E_2)} - \mathrm{atan}\frac{\mathrm{Im}(E_2')}{\mathrm{Re}(E_2')} \tag{22}$$

where E_2' is the note for E_2 after injection. By linearization

$$\Delta\tilde{\theta} = \mathrm{atan}\frac{\mathrm{Im}(E_2)}{\mathrm{Re}(E_2)} - \mathrm{atan}\frac{\mathrm{Im}(E_2')}{\mathrm{Re}(E_2')} = \frac{\mathrm{Im}(E_2)}{\mathrm{Re}(E_2)} - \frac{\mathrm{Im}(E_2')}{\mathrm{Re}(E_2')}. \tag{23}$$

Denote the two terms of the E_2 as

$$E_2 = E_{21} + E_{22}. \tag{24}$$

Since $\Delta\tilde{\theta}$ is very small, and $\tilde{\theta}_1$and $\tilde{\theta}_2$ are so close, $\Delta\tilde{\theta}$ can be calculated by derivatives as

$$\Delta\tilde{\theta} = \frac{\partial\frac{\mathrm{Im}(E_{21})+\mathrm{Im}(E_{22})}{\mathrm{Re}(E_{21})+\mathrm{Re}(E_{22})}}{\partial\boldsymbol{i}_d}\tilde{l}\Delta\boldsymbol{i}_d + \frac{\partial\frac{\mathrm{Im}(E_{21})+\mathrm{Im}(E_{22})}{\mathrm{Re}(E_{21})+\mathrm{Re}(E_{22})}}{\partial\boldsymbol{i}_q}\tilde{l}\Delta\boldsymbol{i}_q$$

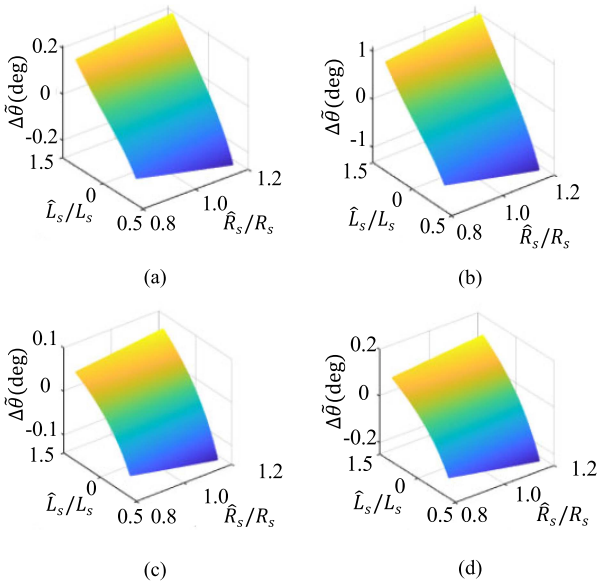

Fig. 4. Estimated rotor position error responses of disturbance current injected. (a) $i_\gamma = 10\%\ i_\delta$, 60000 r/min. (b) $i_\gamma = 50\%\ i_\delta$, 60000 r/min. (c) $i_\gamma = 10\%\ i_\delta$, 30000 r/min. (d) $i_\gamma = 50\%\ i_\delta$, 30000 r/min.

$$\approx \frac{\partial \frac{\mathrm{Im}(E_{21})+\mathrm{Im}(E_{22})}{\mathrm{Re}(E_{22})}}{\partial \boldsymbol{i}_d}\tilde{l}\Delta\boldsymbol{i}_d + \frac{\partial \frac{\mathrm{Im}(E_{21})+\mathrm{Im}(E_{22})}{\mathrm{Re}(E_{22})}}{\partial \boldsymbol{i}_q}\tilde{l}\Delta\boldsymbol{i}_q$$
$$= \frac{1}{\mathrm{Re}\,(E_{22})}\frac{\partial \mathrm{Im}\,(E_{21})}{\partial \boldsymbol{i}_d}\tilde{l}\Delta\boldsymbol{i}_d + \frac{1}{\mathrm{Re}\,(E_{22})}\frac{\partial \mathrm{Im}\,(E_{21})}{\partial \boldsymbol{i}_q}\tilde{l}\Delta\boldsymbol{i}_q$$
$$= \frac{1}{\mathrm{Re}\,(E_{22})}\tilde{l}^2\Delta\boldsymbol{i}_d + \frac{1}{\mathrm{Re}\,(E_{22})}\tilde{l}^2\Delta\boldsymbol{i}_q \tag{25}$$

where $\tilde{l} = \frac{\hat{L}_s - L_s}{\hat{L}_s}$.

Theoretically, $\Delta\tilde{\theta}$ is a infinitesimals with the same order of disturbance. Practically, $\mathrm{Re}(E_{22}) >> 1$ and $\left(\frac{\hat{L}_s - L_s}{\hat{L}_s}\right) < 30\%$, thus $\left(\frac{\hat{L}_s - L_s}{\hat{L}_s}\right)^2 < 0.09$. The coefficients before Δi_d and Δi_q $<< 0.09$. So, it is acceptable to consider $\Delta\tilde{\theta}$ as a higher order infinitesimals with respect to the disturbance Δi_d and neglect the last term in (15). Fig. 4 shows the numerical calculation results of $\tilde{\theta}$ based on the above analytical deducing. Fig. 4(a) and (c) show the responses on the rotor position error when a disturbance i_γ with an amplitude of 10% of i_δ is injected. Fig. 4(b) and (d) show the responses on the rotor position error when a disturbance i_γ with an amplitude of 50% of i_δ is injected. These results indicate that $|\Delta\tilde{\theta}|$ increases as the nominal inductance value deviates from the real value. With a larger $\hat{L}_s$, the estimated rotor position lags in further when - i_γ is injected. However, the deviation of the nominal resistance has little influence on $\Delta\tilde{\theta}$ which allows errors on resistance exist and provides robustness while identifying the inductance.

In above situations, $\Delta\tilde{\theta}$ does not exceed 0.2° when the amplitude of injected i_γ is 10% of the amplitude of i_δ, and hence in this article the amplitude of i_δ injected is smaller than 10%. So, in summary, $\Delta\tilde{\theta}$ is kept small and is negligible.

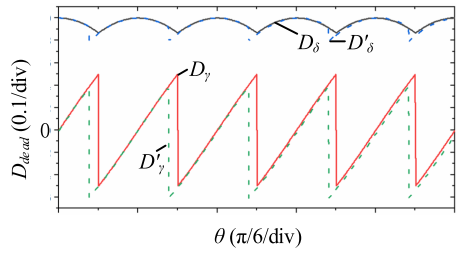

Fig. 5. Waveforms of the DTE equivalent coefficients.

Thus (15) becomes

$$\Delta\boldsymbol{i}_{\gamma\delta} = G\Delta\boldsymbol{i}_{\gamma\delta} + H_d\left(\Delta\boldsymbol{u}_{\gamma\delta} + \Delta\boldsymbol{u}_{\mathrm{dead}_{\gamma\delta}}\right). \tag{26}$$

Equation (26) is independent of back EMF, so that the error in PM flux-linkage will not affect the identification of inductance.

C. Analysis of Dead-Time Effect

Existing research based on conventional models concluded that the DTE has an important influence on the identification. Thus, the influence of DTE on the FOIM is analytically deduced to prove that the FOIM is DTE compensation-free.

The DTE is usually modeled as a DC component with a AC signal of 6 times of fundamental frequency as shown in in Fig. 5. The difference between D_γ, D_δ, D'_γ, D'_δ is shown as follows:

$$\Delta\boldsymbol{u}_{\mathrm{dead}_{\gamma\delta}} = V_{\mathrm{dead}}\left(D_\gamma - D'_\gamma\right) + \mathrm{j}V_{\mathrm{dead}}\left(D_\delta - D'_\delta\right) \tag{27}$$

where V_{dead} is called the equivalent dead time voltage and D_γ, D_δ are the equivalent dead time coefficients, and D'_γ, D'_δ are the equivalent dead time coefficient after disturbance injected. The values of D_γ and D_δ can be calculated as follows:

$$\begin{bmatrix} D_\gamma \\ D_\delta \end{bmatrix} = 2\begin{bmatrix} \cos\left(\hat{\theta}\right) & \cos\left(\hat{\theta} - \frac{2\pi}{3}\right) & \cos\left(\hat{\theta} + \frac{2\pi}{3}\right) \\ -\sin\left(\hat{\theta}\right) & -\sin\left(\hat{\theta} - \frac{2\pi}{3}\right) & -\sin\left(\hat{\theta} + \frac{2\pi}{3}\right) \end{bmatrix} \cdot \mathrm{sign}\left(i_{abc}\right). \tag{28}$$

According to the previous study [27], their average can be calculated as follows:

$$\begin{cases} D_{\gamma_{av}} = 4\sin\left(\vartheta\right) \\ D_{\delta_{av}} = 4\cos\left(\vartheta\right) \end{cases} \tag{29}$$

where $\vartheta = \arctan(i_\gamma / i_\delta)$,then

$$\Delta\boldsymbol{u}_{\mathrm{dead}_{\gamma\delta}} = -4V_{\mathrm{dead}}\left[\sin\left(\arctan\left(\Delta i_\gamma / i_\delta\right)\right)\right] + jV_{\mathrm{dead}}\left[4 - 4\cos\left(\arctan\left(\frac{\Delta i_\gamma}{i_\delta}\right)\right)\right]. \tag{30}$$

With Taylor Expansion

$$\Delta\boldsymbol{u}_{\mathrm{dead}_{\gamma\delta}} = -4V_{\mathrm{dead}}\{\arctan\left(\frac{\Delta i_\gamma}{i_\delta}\right)) + j\left[\sigma\left(\arctan\left(\Delta i_\gamma / i_\delta\right)\right)\right]\} \approx 0 \tag{31}$$

where σ stands for variables which are infinitesimals of the higher order. Since $|\Delta i_\gamma| << |i_\delta|$, $\arctan(\Delta i_\gamma / i_\delta) \approx 0$, then $\Delta \boldsymbol{u}_{\text{dead}_{\gamma\delta}} \approx 0$. Thus, (26) becomes

$$\Delta \boldsymbol{i}_{\gamma\delta} = G\Delta \boldsymbol{i}_{\gamma\delta} + H_d \Delta \boldsymbol{u}_{\gamma\delta} \tag{32}$$

where (32) is DTE compensation-free and independent of PM flux linkage error and rotor position error.

D. Parameter Estimation Method

For the fans and air compressors, surge phenomenon may occur in practice due to the inappropriate load of air pressure. Thus, there could be a low-frequency speed fluctuation with relatively huge amplitude when surge occurs. The speed fluctuation under normal operation is no more than 10 r/min for high-speed sensorless drive. However, when surge occurs the speed fluctuation could be hundreds of rpm which is 30 times of the normal situation. Obviously, it is against the constant-speed assumption in most researches and the identification precision could be reduced. To figure this out, ALSM with forgetting factor is introduced. First, the (32) is a second-order equation set in complex number. Rearrange it in real number form

$$\begin{cases} \Delta i_\gamma = i_{\gamma 2} - i_{\gamma 1}, \Delta i_\delta = i_{\delta 2} - i_{\delta 1} \\ \Delta u_\gamma = u_{\gamma 2} - u_{\gamma 1}, \Delta u_\delta = u_{\delta 2} - u_{\delta 1} \\ \Delta i_{\gamma r} = \Delta i_\gamma \cos(\omega T_s) + \Delta i_\delta \sin(\omega T_s) \\ \Delta i_{\delta r} = \Delta i_\delta \cos(\omega T_s) - \Delta i_\gamma \sin(\omega T_s) \\ \Delta u_{\gamma r} = \Delta u_\gamma \cos(2\omega T_s) + \Delta u_\delta \sin(2\omega T_s) \\ \Delta u_{\delta r} = \Delta u_\delta \cos(2\omega T_s) - \Delta u_\gamma \sin(2\omega T_s) \end{cases}$$

$$x = \frac{\Delta i_\gamma \Delta u_{\delta r} - \Delta i_\delta \Delta u_{\gamma r}}{\Delta i_{\gamma r} \Delta u_{\delta r} - \Delta i_{\delta r} \Delta u_{\gamma r}}$$

$$L_s = -\frac{T_s}{\ln(x)} \hat{R}_s \tag{33}$$

where x is used to form a linear and simple identification model and L_s is calculated from x. The calculation of L_s in (33) is called the FOIM. The nominal value of the resistance is used here instead of the real value for the purpose of order-reduction. By experiments behind, errors of the resistance as large as 30% of the real value has a negligible influence on the inductance estimated. Although at low speed, the mismatch of the resistance parameter will result in a resistive voltage error, it can be compensated easily by calculating the resistance after identifying x by

$$R_s = \frac{(1-x)\Delta u_{\gamma r}}{\Delta i_\gamma - x \Delta i_{\gamma r}}. \tag{34}$$

Since at low speed the SNR of resistive voltage is relatively large, this problem is sufficiently addressed and R_s can be easily obtained [18], [26]. Based on (33), a recursive ALSM with forgetting factor is employed to fit the identification results [18], [28]. The LSM is usually applied in a form of $d = \hat{\omega} u$, where d, u and $\hat{\omega}$ are the output, input and parameters to be estimated

$$\begin{cases} d(n) = \Delta i_\gamma(n) \Delta u_{\delta r}(n) - \Delta i_\delta(n) \Delta u_{\gamma r}(n) \\ u(n) = \Delta i_{\gamma r}(n) \Delta u_{\delta r}(n) - \Delta i_{\delta r}(n) \Delta u_{\gamma r}(n) \\ \hat{\omega}(n) = x(n) \end{cases}. \tag{35}$$

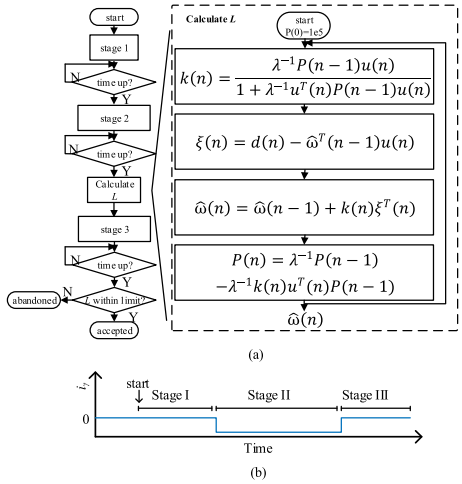

Fig. 6. Diagram of the identification algorithm.

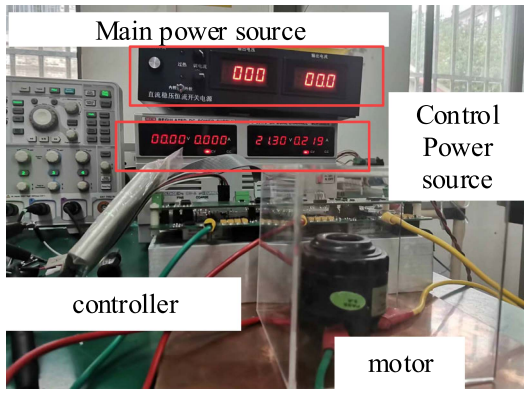

Fig. 7. Experiment platform for high-speed motor drive.

The calculation process is as

$$\begin{aligned} k(n) &= \frac{\lambda^{-1}P(n-1)u(n)}{1+\lambda^{-1}u^T(n)P(n-1)u(n)} \\ \xi(n) &= d(n) - \hat{\omega}^T(n-1)u(n) \\ \hat{\omega}(n) &= \hat{\omega}(n-1) + k(n)\xi^T(n) \\ P(n) &= \lambda^{-1}P(n-1) - \lambda^{-1}k(n)u^T(n)P(n-1) \end{aligned} \tag{36}$$

where the (n) and (n-1) stand for the variables at (n-1)th and nth calculation, k and ξ are, respectively, called the gain and priori estimate error and $\lambda \in [01]$ is the forgetting factor. When $\lambda = 1$, it is the ordinary LSM. However, to deal with the "data saturation" problem, λ usually takes a value between 0.95∼1 by trial-and-error method. Larger λ usually suppresses the fluctuation of the identification results to a lower level while a smaller λ usually tracks the change of the parameter to be identified faster. In this article, $\lambda = 0.98$ to reach a balance between noise rejection and dynamic performance.

The diagram of the identification algorithm is given in Fig. 6(a), and three stages are explained in Fig. 6(b).

TABLE I
KEY PARAMETERS OF THE SPMSM

Parameters	values
Pole pairs	1
rotation speed	60 000 r/min
DC bus voltage	18 V
Rated current	14.85 A
Phase resistance	0.025 Ω
Phase inductance	11.55 μH
Switching frequency	15 kHz

Stage 1, $i_\delta = 0$, wait for steady state. Then record the data before injection.

Stage 2, $i_\delta = -\Delta i_\delta$, wait for new steady state. Then record the data after injection.

Stage 3, $i_\delta = 0$, estimate and change L_s. wait for the update process of the L_s.

The equation of the injected signal is as follows:

$$i_{\text{in}j}(t) = \begin{cases} 0 & t \in \text{Stage I} \\ -\Delta i_\gamma & t \in \text{Stage II} \\ 0 & t \in \text{Stage III} \end{cases}. \tag{37}$$

IV. EXPERIMENTAL VALIDATIONS

Based on the above discussion, experiments are carried out on a prototyped SPMSM with the rated speed of 60 000 r/min. The machine parameters and the platform is shown in Table I as well as in Fig. 7.

A. Test Condition and Initial Parameter Settings

1) *Injection Current Selection*: The Injection current amplitude is decided both by identification models and current measurement noise. In a recent study [20], the multistep injected current steps from 12.5% to 37.5% of q-axis current. Also, in another study [19], the injected current is about 18% of q-axis current. If the model SNR is high enough, the injected current can be as low as 1.33% of q-axis current [17]. The current noise of this experiment platform is about 0.08 A. To let the injected current to be about 15 times of the current measurement noise error, the injected current is set as -1.5A (7.14% of q-axis current), to get an objective presentation of the identification precision of the proposed algorithm. Also, the injected current is set as -0.5 A at light load to evaluate the identification effect under a light load.
2) Switching frequency selection. As the rotation speed is 60 000 r/min, the switching frequency is fixed as 15 kHz. The minimum ratio of carrier-to-fundamental-frequency is selected to be 15.
3) Initial parameters settings. To show the FOIM which derived from disturbance injection is independent of the initial operation point, the initial nominal values largely deviate from the real value. $\hat{L}_{s0}$ is selected as 169.6% and 71.4% of the real value, and $\hat{R}_s$ is 60% and 140% of the real value respectively. So, there are four matches of the initial parameters: $\hat{R}_s = 140\%R_s,\ \hat{L}_s = 170\%L_s$; $\hat{R}_s = 60\%R_s,\ \hat{L}_s = 170\%L_s$; $\hat{R}_s = 60\%R_s,\ \hat{L}_s = 70\%L_s$; and $\hat{R}_s = 140\%R_s,\ \hat{L}_s = 70\%L_s$

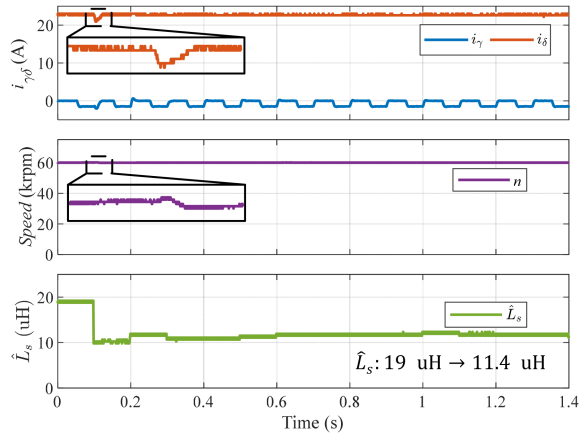

Fig. 8. Identification waveforms. ($\hat{R}_s = 140\%R_s$, $\hat{L}_s = 170\%L_s$, injected Δi_γ= -1.5A, $U_{\text{dc}} = 18$V, rotation speed = 60000 r/min, and ALSM, $\lambda = 0.98$).

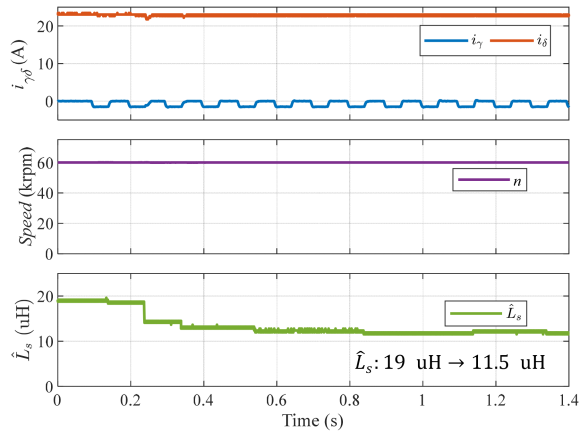

Fig. 9. Identification waveforms ($\hat{R}_s = 60\%R_s$, $\hat{L}_s = 170\%L_s$, injected $\Delta i_\gamma = -1.5$ A, $U_{\text{dc}} = 18$ V, rotation speed = 60000 r/min, and ALSM, $\lambda = 0.98$).

4) The selections of the added speed fluctuation frequency and amplitude. In industrial practice, the surge could cause hundreds of rpm fluctuation of speed with frequency as low as tens of Hertz. So, in this article, the extra added speed reference is a sine-wave with $\pm$200 r/min and 15 Hz.
5) Filter design. As there always exist small fluctuations of variables, a second-order filter is used to get average values of the variables at the steady states before and after injection. The cut-off frequency of the second-order low-pass filter is designed as 100 Hz to allow a fast response.
6) The identification frequency. The whole identification time is 0.1s which is ten times of the time constant of the prefilter in 5). This short-time feature allows the proposed identification method used in most applications.
7) The decision of the real value of the inductance. The real value of the inductance is influential from the real-time temperature of the magnet materials as well as the magnet saturation which is hard to be measured directly online. So, an indirect method is used. First, the average identified inductance under 60 000 r/min is calculated based on the result shown in Figs. 8 –11 which is 11.5 μH. Then, three

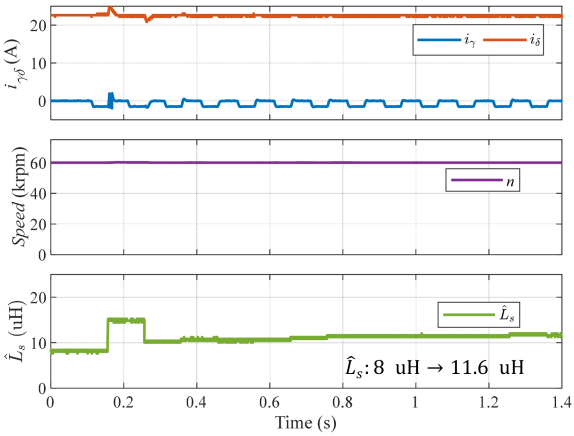

Fig. 10. Identification waveforms ($\hat{R}_s = 60\%R_s$, $\hat{L}_s = 70\%L_s$, injected $\Delta i_\gamma = -1.5$ A, $U_{\rm dc} = 18$ V, rotation speed = 60000 r/min, and ALSM, $\lambda = 0.98$).

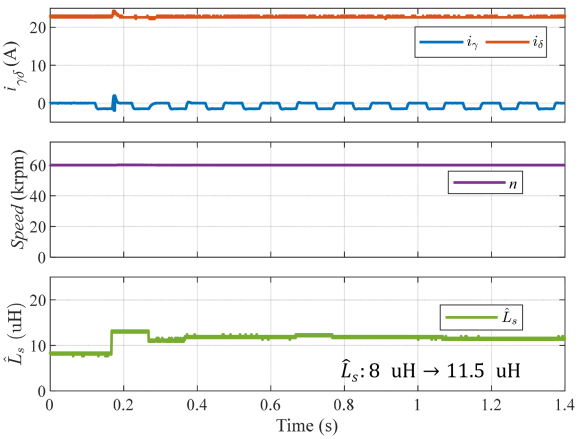

Fig. 11. Identification waveforms ($\hat{R}_s = 140\%R_s$, $\hat{L}_s = 70\%L_s$, injected $\Delta i_\gamma = -1.5$ A, $U_{\rm dc} = 18$ V, rotation speed = 60000 r/min, and ALSM, $\lambda = 0.98$).

extra 40A-rated 22 μH inductors are added in series with the A, B and C windings and the results by Fig. 19 is 33.4 μH. Thus, the identification result for the 22 μH inductors is 33.4–11.5 μH = 21.9 μH and the error for the extra added inductors is (21.9–22 μH)/22 μH = −0.45%. It is worth to notice that the nominal value 22 μH is taken as the real value for the inductors because the 40 A rate current is much larger than the phase current thus the magnet saturation is not considered. Finally, the -0.45% is also approximately considered as the identification error for the L_s and the real value for the L_s is 11.5·(1+0.45%) = 11.55 μH.

B. Experimental Results

In Figs. 8–11, a γ-axis current of −1.5 A is injected. The initial nominal values are shown, respectively. After injection, the disturbance of γ-axis current is removed and the identified inductance value is updated for control. So, there is a current peak of i_δ as a dynamic process.

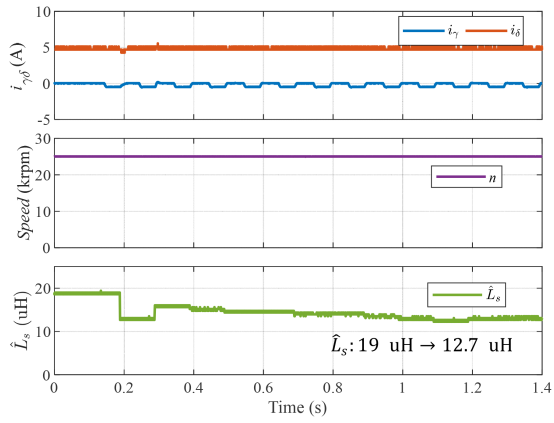

Fig. 12. Identification waveforms ($\hat{L}_{s0} = 170\%\ L_s$, $\hat{R}_s = 60\%R_s$, injected $\Delta i_\gamma = -0.5$ A, $U_{\rm dc} = 18$ V, rotation speed = 25000 r/min, and ALSM, $\lambda = 0.98$).

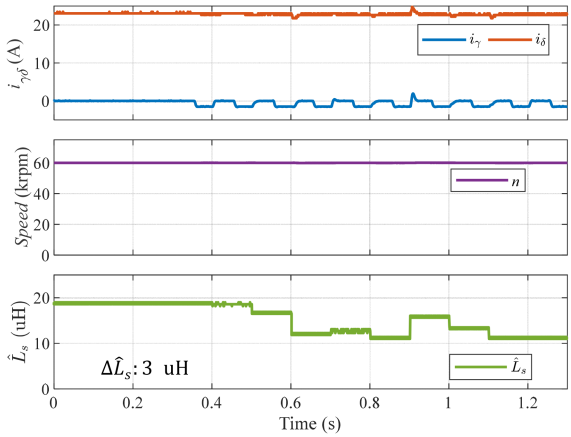

Fig. 13. Identification waveforms ($\hat{L}_{s0} = 170\%\ L_s$, $\hat{R}_s = 60\%R_s$, injected $\Delta i_\gamma = -1.5$A, $U_{\rm dc} = 18$ V, rotation speed = 60000 r/min, without ALSM).

After the first identification, the identified value is not the real value yet. As the identification continues, the identified inductance reaches the real value eventually. The waveform of the rotation speed in detailed subplot also shows the dynamic process. The errors of the four above is all within 1.3%.

Fig. 12 shows the identification when the speed is set as 25 000 r/min to validates the feasibility of the proposed FOIM under light load. The load is a shaft with fans, so the q-axis current amplitude is proportional to the square of rotation speed. Lower rotation speed is not tested because the current will be too small then. The identified inductance converges to 12.8 μH which is larger than the 11.1 μH at 60 kr/min. This is because of the magnet saturation change.

To compare the effect of ALSM, Fig. 13 shows the waveforms without ALSM. There exists violent fluctuation in the identification results (between 11 to 14 μH). In contrast, with ALSM the fluctuation of the identified inductance stays under 1%.

Fig. 14 is the results when conventional continuous-time identification model is used with DTE compensation.

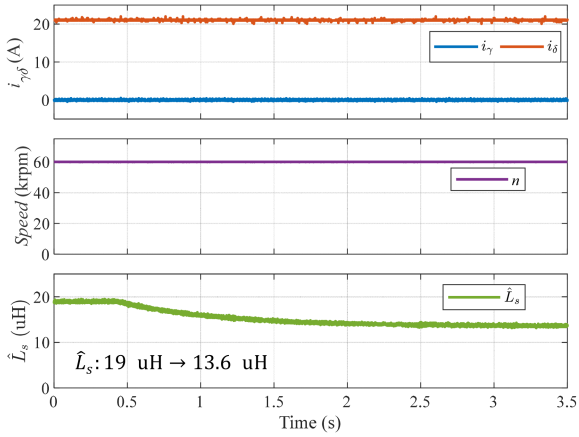

Fig. 14. Identification waveforms of conventional method based on continuous-time model ($\hat{L}_{s0} = 170\%L_s$, $\hat{R}_s = R_s$, $U_{\rm dc} = 18$ V, rotation speed = 60000 r/min, with ALSM).

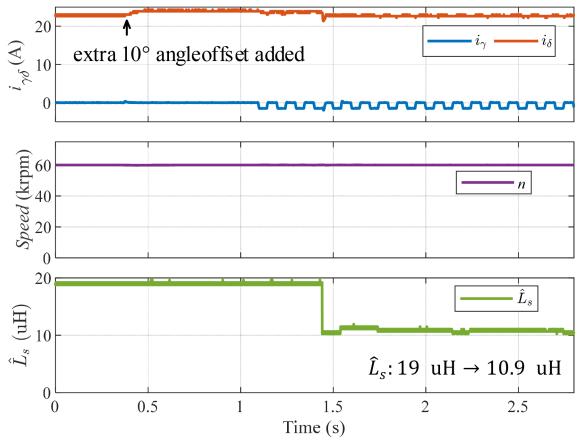

Fig. 15. Identification waveforms ($\hat{L}_{s0} = 170\%L_s$, $\hat{R}_s = 70\%R_s$, $U_{\rm dc} = 18$ V, rotation speed = 60 kr/min, extra 10° lag added, with ALSM).

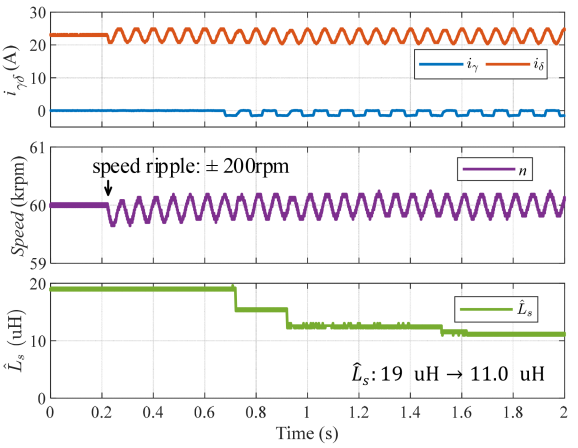

Fig. 16. Identification waveforms ($\hat{L}_{s0} = 170\%L_s$, $\hat{R}_s = 60\%R_s$, $U_{\rm dc} = 18$ V, rotation speed = 60 kr/min, ±200 r/min speed fluctuation added, with ALSM).

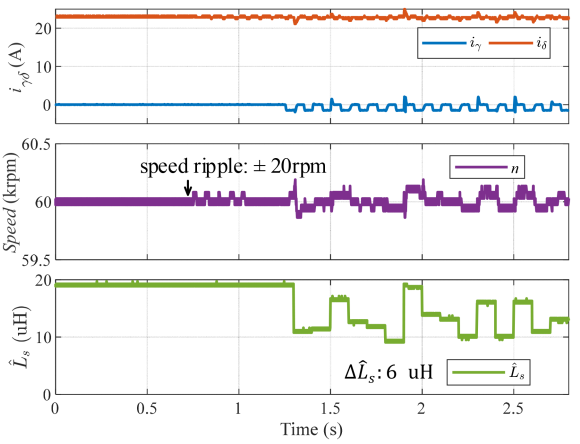

Fig. 17. Identification waveforms. ($\hat{L}_{s0} = 170\%L_s$, $\hat{R}_s = 60\%R_s$, $U_{\rm dc} = 18$ V, rotation speed = 60 kr/min, ±40 r/min speed fluctuation added, without ALSM).

In continuous model, the inductance can be simply calculated as

$$L_q = \frac{[u_d]_{av}}{[-i_q\omega]_{av}}. \tag{38}$$

To avoid the adverse impact of the other uncertainties, the DTE equivalent voltage is test and obtained offline and the actual inductance parameter used in controller is 11.55 μH, which is the real value. Thus, the initial position error is diminished and the identification is simplified as a first-order one. The identification error is huge (17.7%), and it is mainly because of the computational delay and PWM effect which are not modeled in continuous-time model.

Fig. 15 shows the identification results when an extra 10° rotor position error is added. It is designed to show that the proposed identification method is independent of the position error and is thus robust. With a large initial inductance value, the estimated rotor position is about 10° lagged already. After the extra angle added, the whole position error nearly reaches 20°. With the proposed FOIM, the identified inductance value still converges to real value. The results show that large as a 10° angle offset is, the precision of the identification method based on disturbance injection still kept unaffected.

As mentioned in Section III, the surge could result in a relatively large fluctuation in rotation speed which is against the constant-speed assumption in most researches. And the low-frequency disturbance by surge is hard to be filtered. For example, a 15 Hz surge can be considered filtered completely by a low-pass filter with cut-off frequency of several Hertz. However, with that low cut-off frequency, the dynamic will be very slow and the whole identification time could be several seconds to tens of seconds which is too long. Fig. 16 shows the identification results with speed fluctuation. A ±200 r/min 15 Hz speed fluctuation is added and the fluctuation of current reaches 20% then. The ALSM helps the inductance nominal value converges to real value with a 4.9% error.

Fig. 17 is the waveforms of the identification when ALSM is not used. The identified inductance value fluctuates dramatically even when the extra added speed fluctuation is only ±20 rpm. By compare with Fig. 16, the small speed fluctuation could cause a huge identification result deviation from real value.

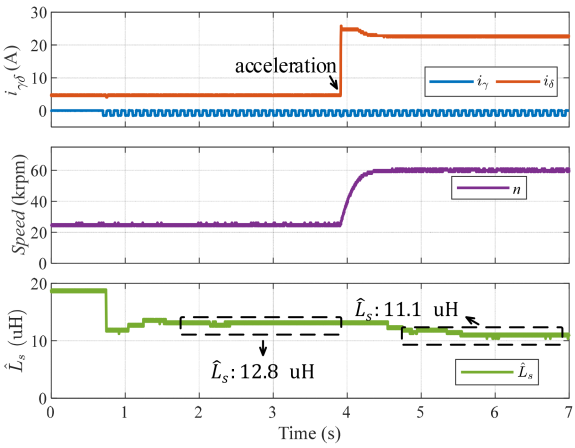

Fig. 18. Identification waveforms ($\hat{L}_{s0} = 170\% L_s$, $\hat{R}_s = 60\% R_s$, $U_{\rm dc} = 18$ V, rotation speed = 25 kr/min step to 60 kr/min, with ALSM).

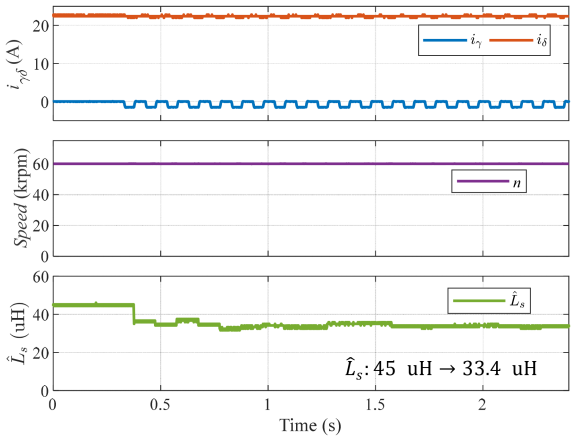

Fig. 19. Identification waveforms ($\hat{L}_{s0} = 130\% L_s$, $\hat{R}_s = 80\% R_s$, $U_{\rm dc} = 18$ V, rotation speed = 60 kr/min, extra 22 μH inductor added, with ALSM).

To show the dynamic performance of the proposed method. The speed is set to step from 25 to 60 kr/min as Fig. 18 shows.

As above, the rotation speed steps form 25 to 60 kr/min in 0.5s. The inductance before stepping is estimated as 12.8 μH, and after stepping the inductance is estimated as 11.1 μH which is due to the magnet saturation. After the load stepping, the estimated inductance tracks the new value in 0.5s which is acceptable in most industrial applications. The real value for the 25 000 r/min case which is 12.86 μH is also obtained in the way same as Section IV-A-7) describes.

As a matter of fact, the real value of the inductance is affected by the real-time temperature of the magnet materials as well as the magnet saturation which is hard to be measured directly online but is essential for identification accuracy analysis. Based on that, Fig. 19 is designed to evaluate the accuracy of the proposed method. It shows the identification results when an extra 22 μH inductor with a 40 A-rated current, which is about 2.8 times of the phase current is added in series with A, B, and C phase windings. The result converges to 33.4 μH after adding those inductors and in contrast, the identified phase stator inductance in Figs. 8–11 is (11.4+11.5+11.6+11.5)/4 = 11.5 μH. The difference is (33.4 μH-11.5 μH) = 21.9 μH, and thus the error is calculated as (21.9 μH-22 μH)/22 μH = -0.45%. Approximately considering the error for the phase stator inductance is the same with the error for the extra added inductors, the real value for the phase inductance is (1+0.45%)·11.5 μH = 11.55 μH.

V. Conclusion

This article develops a first-order model with ALSM for inductance identification to improve the accuracy of estimated position in sensorless control of PMSMs. To avoid the robustness problem brought by conventional high-order models, the proposed FOIM is independent of other parameter uncertainties, namely, PM flux linkage error, initial position error and equivalent DTE voltage. Also, it guarantees the applicability without using any information from back-EMF observer, so the FOIM is compatible with position-sensed situations although it is proposed for sensorless control. To be precise for high-speed motor, the FOIM is deduced on the discrete-time model and computational delay and PWM effect is compensated. To maintain the identification precision under speed fluctuation, the LSM is employed to estimate the inductance. Finally, the proposed FOIM is tested on a SPMSM with a speed of 60 000 r/min. The estimated $\hat{L}_s$ can converge to real value even when initial position error exceeds 20° or a ±200 r/min speed fluctuation is added.

References

[1] G. Wang, M. Valla, and J. Solsona, "Position sensorless permanent magnet synchronous machine drives—A review," *IEEE Trans. Ind. Electron.*, vol. 67, no. 7, pp. 5830–5842, Jul. 2020, doi: 10.1109/TIE.2019.2955409.

[2] H. Kim, J. Son, and J. Lee, "A high-speed sliding-mode observer for the sensorless speed control of a PMSM," *IEEE Trans. Ind. Electron.*, vol. 58, no. 9, pp. 4069–4077, Sep. 2011, doi: 10.1109/TIE.2010.2098357.

[3] J. Kim, I. Jeong, K. Nam, J. Yang, and T. Hwang, "Sensorless control of PMSM in a high-speed region considering iron loss," *IEEE Trans. Ind. Electron.*, vol. 62, no. 10, pp. 6151–6159, Oct. 2015, doi: 10.1109/TIE.2015.2432104.

[4] C. J. V. Filho, D. Xiao, R. P. Vieira, and A. Emadi, "Observers for high-speed sensorless PMSM drives: Design methods, tuning challenges and future trends," *IEEE Access*, vol. 9, pp. 56397–56415, 2021, doi: 10.1109/ACCESS.2021.3072360.

[5] Z. Novak and M. Novak, "Adaptive PLL-based sensorless control for improved dynamics of high-speed PMSM," *IEEE Trans. Power Electron.*, vol. 37, no. 9, pp. 10154–10165, Sep. 2022, doi: 10.1109/TPEL.2022.3169708.

[6] S. Dai, J. Wang, Z. Sun, and E. Chong, "Model inaccuracy analysis and compensation of stationary frame-based deadbeat predictive current control for high-speed PMSM drives," *IEEE Trans. Transp. Electrific.*, vol. 8, no. 2, pp. 2654–2666, Jun. 2022, doi: 10.1109/TTE.2021.3134950.

[7] T. Jiang, R. Ni, S. Gu, and G. Wang, "A study on position estimation error in sensorless control of PMSM based on back EMF observation method," in *Proc. 24th Int. Conf. Elect. Mach. Syst.*, 2021, pp. 1999–2003, doi: 10.23919/ICEMS52562.2021.9634511.

[8] Y. Zhang, Z. Yin, C. Bai, G. Wang, and J. Liu, "A rotor position and speed estimation method using an improved linear extended state observer for IPMSM sensorless drives," *IEEE Trans. Power Electron.*, vol. 36, no. 12, pp. 14062–14073, Dec. 2021, doi: 10.1109/TPEL.2021.3085126.

[9] J. Y. Tan, K. Wang, R. W. Cao, and G. Lyu, "Sensorless control of PMSM machine based on improved PLL structure eliminating integral drift of third harmonic back-EMF," in *Proc. 21st Int. Conf. Elect. Mach. Syst.*, 2018, pp. 1686–1690, doi: 10.23919/ICEMS.2018.8549215.

[10] X. Song, J. Fang, B. Han, and S. Zheng, "Adaptive compensation method for high-speed surface PMSM sensorless drives of EMF-based position estimation error," *IEEE Trans. Power Electron.*, vol. 31, no. 2, pp. 1438–1449, Feb. 2016, doi: 10.1109/TPEL.2015.2423319.

[11] B.-H. Bae and S.-K. Sul, "A compensation method for time delay of full-digital synchronous frame current regulator of PWM AC drives," *IEEE Trans. Ind. Appl.*, vol. 39, no. 3, pp. 802–810, May/Jun. 2003, doi: 10.1109/TIA.2003.810660.
[12] S.-C. Yang and G.-R. Chen, "High-speed position-sensorless drive of permanent-magnet machine using discrete-time EMF estimation," *IEEE Trans. Ind. Electron.*, vol. 64, no. 6, pp. 4444–4453, Jun. 2017, doi: 10.1109/TIE.2017.2652364.
[13] Y. Yao, Y. Huang, and F. Peng, "Position sensorless drive of high speed permanent magnet synchronous motor," in *Proc. IEEE Energy Convers. Congr. Expo.*, 2018, pp. 1733–1740, doi: 10.1109/ECCE.2018.8557716.
[14] Y. Yao, Y. Huang, F. Peng, and J. Dong, "A sliding-mode position estimation method with chattering suppression for LCL-equipped high-speed surface-mounted PMSM drives," *IEEE Trans. Power Electron.*, vol. 37, no. 2, pp. 2057–2071, Feb. 2022, doi: 10.1109/TPEL.2021.3108389.
[15] M. Hu, W. Yu, J. Lei, Z. Wu, W. Hua, and Y. Hu, "Sensorless control of a high-speed PMSM with rapid acceleration for air compressors using a high-order extended state observer," in *Proc. IEEE Energy Convers. Congr. Expo.*, 2021, pp. 4781–4787, doi: 10.1109/ECCE47101.2021.9595719.
[16] N. K. Quang, N. T. Hieu, and Q. P. Ha, "FPGA-based sensorless PMSM speed control using reduced-order extended Kalman filters," *IEEE Trans. Ind. Electron.*, vol. 61, no. 12, pp. 6574–6582, Dec. 2014, doi: 10.1109/TIE.2014.2320215.
[17] Y. Yao, Y. Huang, F. Peng, J. Dong, and Z. Zhu, "Compensation method of position estimation error for high-speed surface-mounted PMSM drives based on robust inductance estimation," *IEEE Trans. Power Electron.*, vol. 37, no. 2, pp. 2033–2044, Feb. 2022, doi: 10.1109/TPEL.2021.3106510.
[18] S. Ichikawa, M. Tomita, S. Doki, and S. Okuma, "Sensorless control of permanent-magnet synchronous motors using online parameter identification based on system identification theory," *IEEE Trans. Ind. Electron.*, vol. 53, no. 2, pp. 363–372, Apr. 2006, doi: 10.1109/TIE.2006.870875.
[19] S. Liu, Q. Wang, G. Zhang, G. Wang, and D. Xu, "Online temperature identification strategy for position sensorless PMSM drives with position error adaptive compensation," *IEEE Trans. Power Electron.*, vol. 37, no. 7, pp. 8502–8512, Jul. 2022, doi: 10.1109/TPEL.2022.3149804.
[20] Y. Wang, Y. Xu, and J. Zou, "Online multiparameter identification method for sensorless control of SPMSM," *IEEE Trans. Power Electron.*, vol. 35, no. 10, pp. 10601–10613, Oct. 2020, doi: 10.1109/TPEL.2020.2974870.
[21] Z. Q. Zhu, D. Liang, and K. Liu, "Online parameter estimation for permanent magnet synchronous machines: An overview," *IEEE Access*, vol. 9, pp. 59059–59084, 2021, doi: 10.1109/ACCESS.2021.3072959.
[22] X. Li and R. Kennel, "General formulation of Kalman-filter-based online parameter identification methods for VSI-fed PMSM," *IEEE Trans. Ind. Electron.*, vol. 68, no. 4, pp. 2856–2864, Apr. 2021, doi: 10.1109/TIE.2020.2977568.
[23] N. Hoffmann, F. W. Fuchs, M. P. Kazmierkowski, and D. Schroder, "Digital current control in a rotating reference frame - Part I: System modeling and the discrete time-domain current controller with improved decoupling capabilities," *IEEE Trans. Power Electron.*, vol. 31, no. 7, pp. 5290–5305, Jul. 2016, doi: 10.1109/TPEL.2015.2481726.
[24] H. Kim, M. W. Degner, J. M. Guerrero, F. Briz, and R. D. Lorenz, "Discrete-time current regulator design for AC machine drives," *IEEE Trans. Ind. Appl.*, vol. 46, no. 4, pp. 1425–1435, Jul./Aug. 2010, doi: 10.1109/TIA.2010.2049628.
[25] Z. Chen, M. Tomita, S. Doki, and S. Okuma, "An extended electromotive force model for sensorless control of interior permanent-magnet synchronous motors," *IEEE Trans. Ind. Electron.*, vol. 50, no. 2, pp. 288–295, Apr. 2003, doi: 10.1109/TIE.2003.809391.
[26] Y. Yu et al., "Full parameter estimation for permanent magnet synchronous motors," *IEEE Trans. Ind. Electron.*, vol. 69, no. 5, pp. 4376–4386, May 2022, doi: 10.1109/TIE.2021.3078391.
[27] N. Urasaki, T. Senjyu, K. Uezato, and T. Funabashi, "An adaptive dead-time compensation strategy for voltage source inverter fed motor drives," *IEEE Trans. Power Electron.*, vol. 20, no. 5, pp. 1150–1160, Sep. 2005, doi: 10.1109/TPEL.2005.854046.
[28] Q. Liu and K. Hameyer, "A fast online full parameter estimation of a PMSM with sinusoidal signal injection," in *Proc. IEEE Energy Convers. Congr. Expo.*, 2015, pp. 4091–4096, doi: 10.1109/ECCE.2015.7310237.

Yinfeng Hu received the B.Sc. degree in electrical engineering from the School of Electrical and Electronic Engineering, Huazhong University of Science and Technology, Wuhan, China in 2018, and the Master's degree from the College of Automation Engineering, Nanjing University of Aeronautics and Astronautics, Nanjing, China in 2021. He is currently working toward the Ph.D. degree in high-speed motor drive and advanced current control with the School of Electrical Engineering, Southeast University, Nanjing, China.

His current research interests include power electronics and motor drive.

Kai Liu received the B.Sc., M.Sc., and Ph.D. degrees in electrical engineering from the Harbin Institute of Technology, Harbin, in 2005, 2007, and 2014, respectively.

Since 2015, he has been with Southeast University, where he is currently a Lecturer with the School of Electrical Engineering. His teaching and research interests include control of electrical machines and flywheel energy storage systems.

Wei Hua (Senior Member, IEEE) received the B.Sc. and Ph.D. degrees in electrical engineering from Southeast University, Nanjing, China, in 2001 and 2007, respectively.

From 2004 to 2005, he was with the Department of Electronics and Electrical Engineering, The University of Sheffield, Sheffield, U.K., as a Joint-Supervised Ph.D. Student. His teaching and research interests include design, analysis, and control of electrical machines, especially for PM brushless machines and switching reluctance machines, etc.

Mingjin Hu (Student Member, IEEE) received the B.Sc. degree in 2016 in electrical engineering from the School of Electrical Engineering, Southeast University, Nanjing, China, where he is currently working toward the Ph.D. degree in electrical engineering.

His current research interests include the modeling and advanced control of electrical machines.